Chapter 5

GRB 050401 : A case for a Double Jet Model

Abstract

The afterglow of GRB 050401 presents several novel and interesting features. We have modeled the observed multi-band evolution of the afterglow of GRB 050401 as originating in a two component jet, interpreting the break in x-ray light curve as being due to lateral expansion of a narrow collimated outflow which dominates the x-ray emission. The optical emission is attributed to a wider jet component. Our model reproduces all the observed features of multi-band afterglow of GRB 050401. We present optical observations of GRB 050401 using the 104-cm Sampurnanand Telescope at ARIES, Nainital. We also present a re-analysis of the x-ray data of GRB 050401 taken by *Swift*-XRT. Results of the analysis of multi-band data are presented and compared with GRB 030329, the first reported case of double jet.

5.1 Introduction

The optical and x-ray light curves of Gamma Ray Burst (GRB) afterglows, in the simplest cases, show a power law decay with an index $\alpha \sim 1.0$. Deceleration of the relativistic shock wave generated by the explosion which results in GRB can explain the power law decay of the GRB afterglows. The most common deviation from the power law decay behaviour of the afterglow light curves is an achromatic break seen in the light curve. This break has been seen in a significant number of GRB afterglows and has been successfully explained as being due to the sideways expansion of the collimated ejecta from the explosion. In the post *Swift* era, many more deviations from this simple behaviour of the afterglow light curve have been detected. *Swift* with its capabilities of quick slewing towards the source has been able to observe GRB afterglows as early as a tens of seconds after burst. In this early part of the evolution the GRB afterglows commonly exhibit a steep decay with $\alpha \sim$ 3 to 5 with the usual definitions $F_\nu(t) \propto t^{-\alpha}\nu^{-\beta}$ where $F_\nu(t)$ is the observed afterglow flux at frequency 'ν' and time 't'. The phase of steep decay lasts for about a few hundred seconds after which a slower decay, with $\alpha \sim 0.5$, of the afterglow starts. After about a few thousands of seconds after the burst the afterglow starts decaying steeply again with $\alpha > 1.0$.

Many GRB afterglows observed by *Swift* show puzzling features in the light curves like (1.) early steep decay [$\alpha \sim 3$ *to* 5] and (2.) Chromatic breaks (breaks seen in some wavebands but not others) with $\Delta\alpha \sim 1.0$ which are difficult to explain using the standard fireball model (Rees and Meszaros, 1992; Meszaros and Rees, 1993). It has been shown by O'Brien et al. (2006); Willingale et al. (2006) that the puzzling features of the x-ray afterglow light curves can be fitted using one or two components with exactly the same empirical functional form, viz. an exponential fall followed by a powerlaw decay of flux with time, although it has not yet resulted

into any physical understanding of the behaviour of the x-ray afterglow. While there is no clear understanding of the early steep decays of GRB afterglows, a few plausible explanations have been put forward : see e.g. (Zhang et al., 2006; Pe'er et al., 2006). The flat decay of x-ray afterglow light curves which follows the steep decay have been, in some cases, explained as being due to energy injection from the central engine, probably a magnetar (Zhang and Mészáros, 2001, 2002). From the study of chromatic breaks seen in six well sampled afterglow light curves Panaitescu et al. (2006) concludes that if both, the optical and the x-ray afterglows, were to arise from the same outflow then the chromaticity of light curve breaks can rule out energy injection or the structure of the jet as the possible reasons of it. From the lack of spectral evolution across the break time Panaitescu et al. (2006) further concludes that they do not arise due to the passage of any spectral break.

One such GRB afterglow with puzzling features in optical and x-ray light curves is GRB 050401. *Swift*-BAT triggered GRB 050401 at 14:20:15 UT on 2005 April 01 (Barbier et al., 2005). *Swift*-XRT found a bright source located at $\alpha = 16^{h}31^{m}29^{s}$ and $\delta = +02^{\circ}11^{'}14^{''}$ (J2000) (Angelini et al., 2005) with an uncertainty of about $6^{''}$. The optical afterglow candidate was later confirmed by ground based observations by Price and McNaught (2005). Refined analysis of the BAT data showed that the burst had four distinct peaks (Sakamoto et al., 2005). The burst duration T_{90} is estimated to be $\sim$ 33 seconds. The fluence as estimated from the analysis of the BAT data in 15-150 keV band was $\sim 10^{-5}$ erg cm^{-2} (De Pasquale et al., 2006). Simultaneously, Konus-Wind also detected the GRB in 0.02-20 MeV band with a fluence $1.93 + / - 0.04 \times 10^{-5}$ erg cm^{-2} (Golenetskii et al., 2005). The photon index of the time-averaged spectrum is 1.50 ± 0.06 (Sakamoto et al., 2005). On 2005 April 02, Fynbo et al. (2005) obtained the spectrum of the afterglow of GRB 050401 and detected several absorption lines. The redshift of GRB 050401

is measured to be z = 2.9 (Fynbo et al., 2005). At this redshift, the isotropic equivalent energy of the explosion released in gamma rays estimated using the fluence reported by Golenetskii et al. (2005) amounts to 1.4×10^{54} erg for a flat universe with $\Omega_m = 0.3, \Omega_\Lambda = 0.7$ and $H_0 = 70$ km s^{-1} Mpc^{-1}.

Multiband afterglow of GRB 050401 also presents some puzzling features which can be summarised as follows :

1. An initially faster decay in optical band than in x-rays.

2. A break in the x-ray light curve after ~ 0.05 day with an unusual slope after the break. The x-ray afterglow does not show any spectral evolution across the break.

3. The R band light curve does not show any noticeable steepening, during the span of observations.

4. Overall flatter decay compared to the general population of GRB afterglows.

In § 5.2 of this Chapter, we present a re-analysis of the x-ray observations of GRB 050401 afterglow. The optical observations are presented in § 5.3. We have done some preliminary analysis of the light curves which is discussed in § 5.4. We have tried to explain the multi-band behaviour of the GRB afterglow using a double jet model which is described in § 5.5 along with the previous attempts by others using a different model. In the Discussion section (§ 5.6), intervening molecular clouds as a plausible explanation for the large extinction is presented (§ 5.6.1). The only other GRB afterglow which has been explained using a similar double jet model is the GRB 030329 (Berger et al., 2003; Resmi et al., 2005). We compare the physical features of GRB 030329 and GRB 050401 in § 5.6.2. In § 5.6.3 we discuss the Ghirlanda relation in the context of our interpretation of the early x-ray break

as being a jet break and the resultant estimates of collimation corrected energy of GRB 050401. Our conclusions are summarised in § 5.7.

5.2 Analysis of *Swift* XRT data

We performed the analysis of the XRT data using XRT pipeline software. XRT WT mode preserves one dimensional information about the images. For extracting counts from WT mode images we used a rectangular box of size 60×40 pixels. The box was centred on the source position for extraction of source counts and away from the source position for extraction of background counts. Only those events which fall between 0-2 grade for WT mode were extracted. For PC mode counts extraction, circular regions of 20 and 60 pixel radius, centred on the source position, were used for source and background respectively. The 60 pixel radius circular region centred on the source position, actually has 'source + background' counts. To extract only background counts from this region, we subtracted counts from the source region. In PC mode, events with grades 0-12 were extracted.

For spectral analysis, ancillary response files (ARFs) were generated using task XRTMKARF. We used Response Matrix Files (RMFs) retrieved from *Swift* Calibration database CALDB 20060427. We binned the data in energy with a condition of having at least 20 counts per bin. This was performed using task GRPPHA.

The x-ray light curve shows a break at ~ 0.05 days. WT and PC mode observations span a period across the break. Hence, we separated data into two temporarily distinct regions : pre-break and post-break. PC mode data in the pre-break region is piled up and we did not include this data into the analysis. Spectral analysis was performed on the rest of the pre-break and post-break data using software XSPEC. The x-ray spectra shows absorption at low energies (0.2-1.0

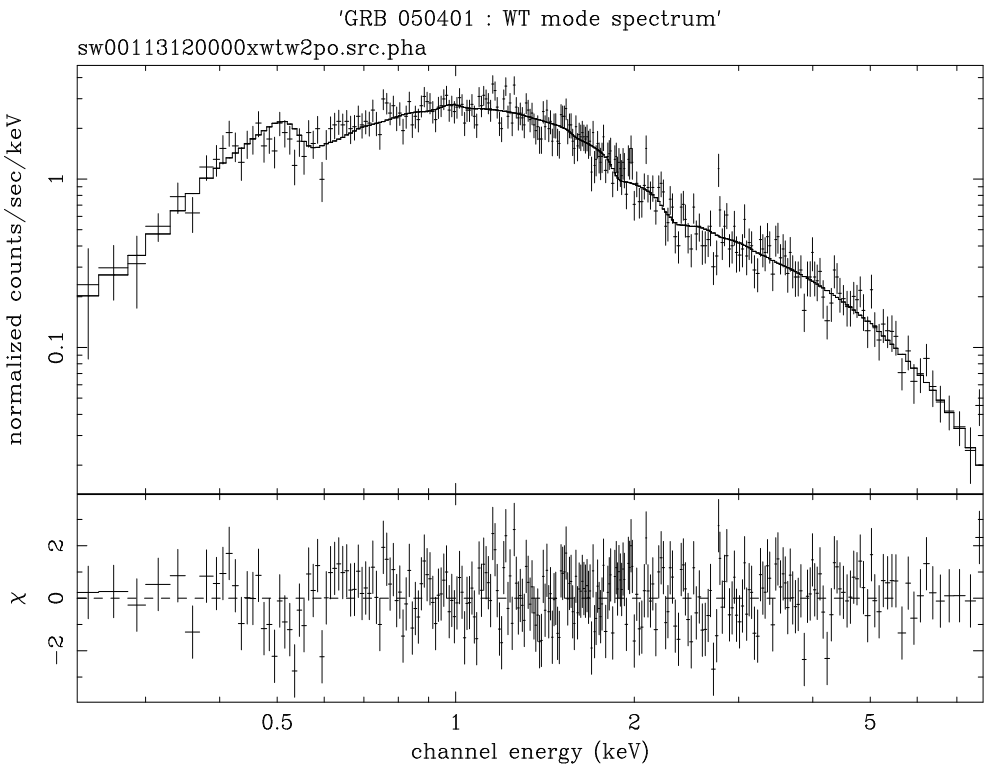

Figure 5.1: *Swift*-XRT observations of GRB 050401. The WT mode spectrum before the break in x-ray light curve at 0.07 day. Spectrum of GRB 050401 is well described by 'absorbed power law' model. Best fit parameters for this model are listed in Table 5.1

keV) then it peaks around 1.0 keV and falls off at higher energies. We fitted 'absorbed power law' to these spectra. The results of these spectral fits are listed in Table 5.1. An important thing one notices from these fits besides excessive absorption ($N_H > 10^{21} cm^{-2}$) is that the spectrum does not change across the break seen in the x-ray light curve. Best fit 'absorbed power law' model is plotted in Figure 5.1.

We used events from within 1.0 to 10 keV spectral range using WT and PC mode data to construct the x-ray light curve.

section	Mode	Photon Index	$N_H(10^{22})$	χ^2_ν
pre-break	WT	2.1 ± 0.05	1.7 ± 0.1	277/281
post-break	WT	2.1 ± 0.2	1.2 ± 0.5	10/25
post-break	PC	1.8 ± 0.3	$1.1^{+0.7}_{-0.6}$	12/17

Table 5.1: Analysis of *Swift* XRT observations of GRB 050401. Spectral parameters are determined using XSPEC. Pre-break and post-break sections in column 1 corresponds to data before and after 0.05 day since burst where x-ray light curve shows a break. Pre-break PC mode data is piled up and hence it is not included in this analysis.

5.3 Optical Observations and Data Reduction

Optical observations of the afterglow of GRB 050401 were carried out in the broad and Johnson V and Cousins RI filters using the 104-cm Sampurnanand Telescope of ARIES, Nainital on 01 April 2005. The gain and read out noise of the CCD camera are 10 e^-/ADU and 5.3 e^- respectively. The data have been binned in 2×2 pixel^2 to improve the signal-to-noise ratio. The bias subtracted, flat fielded and cosmic ray removed images were processed and analysed using MIDAS [1], IRAF [2] and DAOPHOT (Stetson, 1987) softwares.

The Landolt (1992) standard region SA 107 and the OA field in BVRI filters was observed on 16 May 2005 for photometric calibration during good photometric sky conditions. The values of atmospheric extinction on the night of 16/17 May 2005 determined from the observations of SA 107 bright stars are 0.26, 0.18, 0.13 and 0.10 magnitude in B, V, R and I filters respectively. The 7 standard stars in the SA 107 region cover a range of $0.339 < (V - R) < 0.923$ in color and $12.116 < V < 14.884$ in brightness.

Using these transformation coefficients we determine BVRI magnitudes of

[1]MIDAS is distributed by the European Southern Observatories. Visit : www.eso.org/esomidas/

[2]IRAF is distributed by the National Optical Astronomy Observatories, USA. Visit : http://iraf.noao.edu/

18 secondary stars in GRB 050401 field and their average values are listed in Table 5.2. The (X, Y) CCD pixel coordinates were converted to α_{2000}, δ_{2000} values using the astrometric positions given by Henden (2005). The 18 secondary stars in the field of GRB 050401 were observed 2 to 4 times in B, V, R and I filters. These stars have internal photometric accuracy better than 0.01 mag. The zero-point differences on comparison between our photometry and that of Henden (2005) are 0.15 ± 0.08, 0.09 ± 0.04, 0.10 ± 0.05 and 0.54 ± 0.29 magnitude in B, V, R and I filters respectively. These differences are based on the comparison of the 6 secondary stars in the GRB 050401 field.

The afterglow magnitudes were differentially calibrated with respect to the secondary stars listed in Table 5.2. The magnitudes derived in this way are given in Table 5.3.

5.4 Light curves of GRB 050401 afterglow

Along with our own observations we have used observations reported elsewhere to study the light curves of GRB 050401.The optical observations by Watson et al. (2005) have been calibrated by observing a Landolt field. We do not have a detailed information about this calibration. Another set of optical observations is taken from Rykoff et al. (2005) the calibration of which is roughly equivalent to the R_c band system. To take into account any uncertainties associated with calibration of these datasets, we have doubled the quoted uncertainties. We have confirmed that this does not significantly alter the values of the fitted parameters.

VLA reported a 4σ detection of a source at the position of GRB 050401 (Soderberg, 2005) with intensity of 122 μJy at 8.46 GHz about 5.7 days after the burst. Other attempts, including by GMRT in India at 610 MHz (Chandra and Ray, 2005) and by ATCA in Australia at 8.5 GHz and 4.8 GHz (Saripalli et al., 2005),

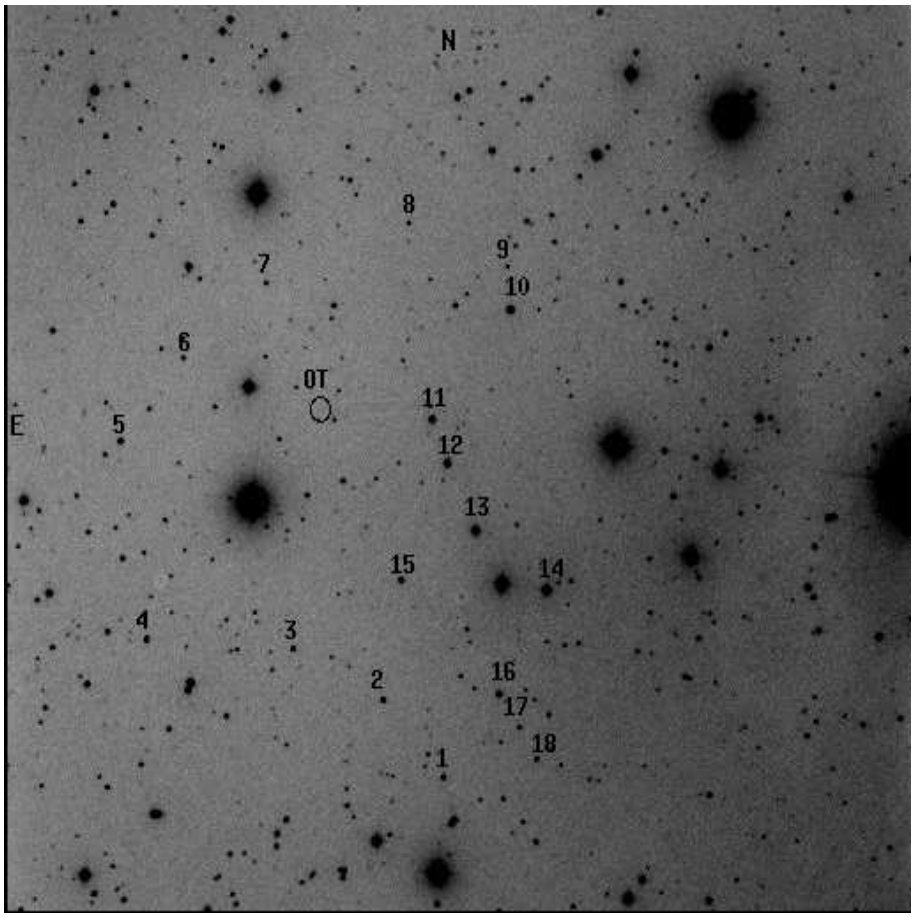

Figure 5.2: I band image of GRB 050401 optical afterglow obtained using the 104-cm ST at ARIES, Nainital. The position of the optical afterglow is marked with a circle. Also marked are the 18 secondary stars used for calibration. North is up and East is to the left.

ID	α_{2000} (h m s)	δ_{2000} (deg m s)	V (mag)	$B-V$ (mag)	$V-R$ (mag)	$V-I$ (mag)
1	16 31 20.01	02 06 52.9	17.28	0.64	0.35	0.84
2	16 31 23.84	02 07 44.3	16.87	0.77	0.52	0.98
3	16 31 29.22	02 08 13.8	17.66	1.14	0.75	1.40
4	16 31 37.63	02 08 07.3	16.78	0.69	0.46	0.87
5	16 31 40.12	02 10 30.1	16.35	0.58	0.38	0.73
6	16 31 36.96	02 11 36.5	18.23	0.97	0.62	1.12
7	16 31 32.61	02 12 38.7	17.68	0.41	0.34	0.67
8	16 31 24.79	02 13 35.4	19.56	1.37	1.08	2.29
9	16 31 18.94	02 13 12.1	19.21	1.26	0.83	1.60
10	16 31 18.56	02 12 40.8	15.30	0.85	0.51	0.93
11	16 31 22.46	02 11 13.7	15.61	0.69	0.46	0.87
12	16 31 21.38	02 10 43.0	15.51	0.88	0.53	0.99
13	16 31 19.42	02 09 56.3	14.60	0.55	0.36	0.69
14	16 31 15.08	02 09 19.1	14.34	0.61	0.38	0.74
15	16 31 23.42	02 09 13.7	16.39	0.66	0.44	0.83
16	16 31 17.26	02 07 58.9	16.17	0.63	0.41	0.81
17	16 31 15.93	02 07 36.6	18.91	1.16	0.89	1.75
18	16 31 14.79	02 07 14.6	17.54	0.74	0.47	0.93

Table 5.2: The identification number (ID), (α, δ) for epoch 2000, standard V, ($B-V$), ($V-R$) and ($V-I$) photometric magnitudes of the stars in the field of GRB 050401. See Figure 5.2

Date (UT) 2005 April	ΔT (days)	Magnitude (mag)	Passband
01.8824	0.2850	22.33 ± 0.347	V
01.8324	0.2850	21.43 ± 0.231	R
01.8698	0.2724	20.51 ± 0.207	I

Table 5.3: The optical observations of the afterglow of GRB 050401 using the 104-cm Sampurnanand Telescope at ARIES, Nainital. ΔT in column 2 refers to the time after the burst in days. The effective exposure time after combining all the images turns out to be 900 *s* for individual passbands reported here.

to observe the radio afterglow of GRB 050401 could produce only upper limits.

To construct the optical light curve we have corrected the observed magnitudes for the standard Galactic extinction law given by Mathis (1990). The Galactic extinction in the direction of GRB 050401 is estimated to be E(B-V) = 0.065 mag from the smoothed reddening map provided by Schlegel et al. (1998). The effective wavelength and normalisation given by Bessell et al. (1998) were used to convert the magnitudes to fluxes in μJy.

Most of the GRB afterglow light curves are well characterised by a broken power law of the form

$$F = F_0\{(t/t_b)^{\alpha_1 s} + (t/t_b)^{\alpha_2 s}\}^{-1/s} \tag{5.1}$$

where α_1 and α_2 are the afterglow flux decay indices before and after the break time (t_b), respectively. F_0 is the flux normalisation and 's' is a smoothening parameter which controls the sharpness of the break. Most known GRB afterglows have $\alpha_1 \sim 1$ and $\alpha_2 > \alpha_1$ i.e. the decay becomes steeper after the break.

The x-ray and optical (R band) afterglow of GRB 050401 is very well sampled over a wide period of observation. The available R band observations cover a duration from 36 s to 13 days after the burst while the x-ray observations range from $\sim$ 130 s to 12 days after the burst. The x-ray afterglow light curve shows a prominent break near 0.06 day while the optical afterglow does not show any such break in the light curve. We analyse this behaviour in detail below.

1. The x-ray light curve shows a clear break near 0.06 day. The change of slope across the break is significant. Fitting Equation 5.1 to the data yield the decay slopes

$$\alpha_{X1} = 0.58 \pm 0.02 \text{ for } \Delta t < 0.06 \text{ day};$$

$$\alpha_{X2} = 1.37 \pm 0.03 \text{ for } \Delta t > 0.06 \text{ day};$$

   The change of slope across the break, $\Delta\alpha_X \sim 0.8$, is therefore quite substantial.

2. The optical afterglow shows a monotonic decay with decay index $\alpha_R = 0.82 \pm 0.02$ over the entire period of observation (up to 13 days). There is no evidence of a break simultaneous with that in the x-ray light curve.

3. According to the standard fireball model of GRB afterglows, the x-ray light curve is expected to decay at least as fast as the optical light curve which is indeed true for the majority of GRB afterglows observed so far. In the case of GRB 050401, we find that the x-ray afterglow shows a decay slower than optical light curve till $\sim$ 0.06 day after which it decays at a much faster rate as described above.

   Thus, the relatively slow initial decay of optical and x-ray light curves, presence of a break in x-ray light curve and absence of such a break in optical, and

initially slower decay of the light curve in x-rays than in optical bands makes the afterglow of GRB 050401 an unusual and interesting one.

5.5 Modeling of GRB 050401 afterglow

The change in slope across the break in the x-ray light curve $\Delta\alpha_X \sim 0.8$ is too large to be explained by the passage of a spectral break. In the standard fireball model of GRB afterglows the passage of the cooling break ν_c through the observing band leads to a steepening of light curve by an amount $\Delta\alpha_X = 0.25$, much smaller than that is observed for GRB 050401 afterglow, along with the change of spectral slope by $\Delta\beta_X = 0.5$. The x-ray spectrum of GRB 050401 does not exhibit any change in the spectral slope across the break. We thus rule out the possibility of ν_c passing through the x-ray band at the time of break.

De Pasquale et al. (2006) explains the initial flatter decay and the break in the x-ray light curve based on a model by Zhang and Mészáros (2001, 2002). According to this model, the central engine of GRB remains active for several thousand seconds after the burst, continuously injecting energy into the fireball. If the central engine is injecting energy above a certain critical rate then it can slow down deceleration of the shock wave which results in a shallow decay of the light curve. The break in the light curve occurs when the central engine stops injecting sufficient amount of energy into the fireball. After this epoch the afterglow can be described using standard fireball model giving $\alpha = (3/2)\beta$. Being a dynamical effect, the end of energy injection episode would result in an achromatic break in the afterglow light curves. Although this model seem to explain the x-ray light curve reasonably well, absence of a similar break in optical afterglow light curve is sufficient to rule this model out for GRB 050401.

Watson et al. (2005) point out another puzzle : the soft x-ray absorption implies an equivalent optical extinction of magnitude $A_v = 9.1^{+1.4}_{-1.5}$ magnitudes in the host galaxy, assuming solar abundance.

However, if the optical and the x-ray emission are part of the same synchrotron spectrum, then A_v is constrained to be ~ 1.45 for no spectral break between optical and x-rays and $A_v < 0.67$ if a cooling break exists in between (an SMC extinction law is assumed). These values are highly discordant with that predicted from x-ray absorption. See Figure 5.3. Watson et al. (2005) suggests that this may indicate either an over abundance of α elements or a non-universal dust to metals ratio.

We consider another possibility. We conjecture that two distinct jet components give rise to the observed emission in these two (x-ray and optical) wavelength bands. The jet contributing to x-ray emission is narrow, exhibiting an early break while that contributing to the optical emission is wider. The optical contribution from the narrow jet is strongly diminished due to the presence of high extinction $A_v \sim 9$ in the line of sight, while the wider jet suffers from a smaller degree of average extinction.

5.5.1 Spectral Parameters of the Afterglow of GRB 050401

The radiation spectrum of a GRB afterglows exhibits a power law spectrum characterised by three break frequencies - the self absorption frequency ν_a, the peak frequency ν_m corresponding to the lower cutoff (γ_m) in the electron energy distribution ($n(\gamma_e) \propto \gamma_e^{-p}$, $\gamma_e > \gamma_m$ where γ_e is the Lorentz factor of the radiating electrons) and the synchrotron cooling frequency ν_c. The flux F_m at ν_m provides the normalisation of the spectrum (Sari et al., 1998).

The photon index (Γ) of the x-ray afterglow is related to its spectral index

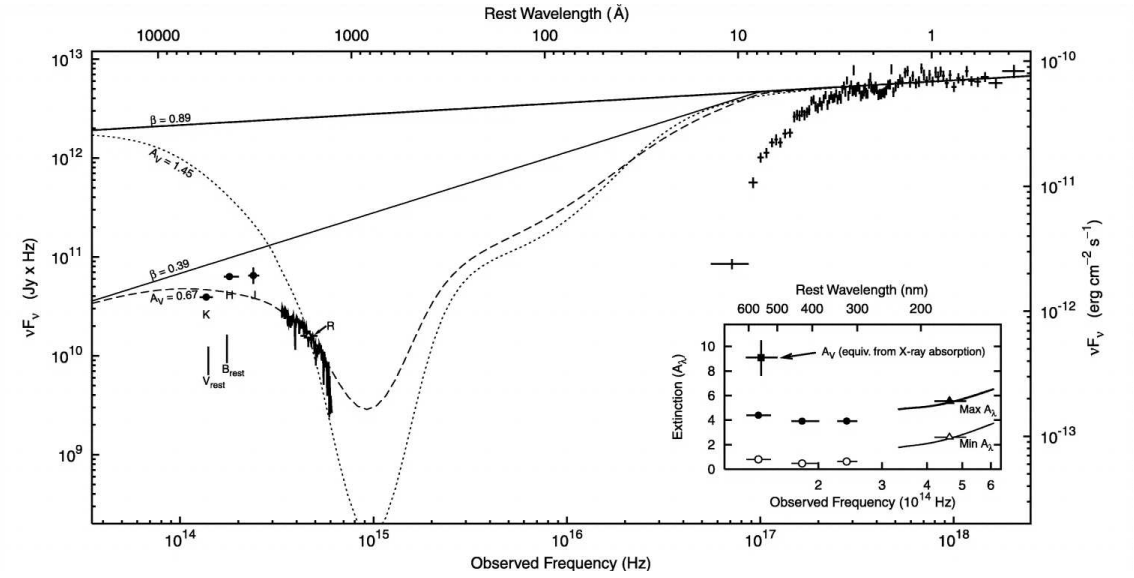

Figure 5.3: SED of the afterglow of GRB 050401. The best-fit single power law ($\beta = 0.89$) to the X-ray data is plotted and extrapolated to optical-NIR wavelengths. All data have been interpolated to a common epoch of 17.9 minutes after the burst using the R-band light curve. There is no evidence for a break in the X-ray power-law spectrum. To derive the minimum extinction required to dim the extrapolated X-ray power law to the fluxes observed in the optical-NIR, the most conservative likely broken power law ($\beta = 0.39$) is also plotted, with the break set at as high an energy as possible, at 0.4 keV (setting the break at lower energies requires larger extinction, while a higher break energy is ruled out by the x-ray spectrum). Fitting SMC extinction to the optical continuum spectrum (rebinned here by a factor of 10) assuming an underlying $\beta = 0.39$ broken power law, gives a good fit with $A_V = 0.67$ and is plotted as a dashed line. The SMC extinction that would be required to account for the R-band photometric data, assuming the single power-law ($\beta = 0.89$) continuum extrapolated from the x-rays, is $A_V = 1.45$, and this is plotted as a dotted line for comparison. However, this is clearly not compatible with the observed optical spectral shape. Inset: Maximum and minimum extinctions as a function of wavelength. These limits for the total extinction are derived from the single and broken power laws ($\beta = 0.89$ and 0.39 outlined above) divided by the observed data. Circles represent the observed NIR data, triangles represent the observed R band, and the solid curve represents the continuum from the spectral observations. By contrast, the extinction expected from the soft x-ray absorption measurement is plotted as a filled square. The inconsistency of the optical/NIR limits with the extinction expected from the x-ray absorption shows that there is no room in the SED to allow for a total extinction that matches the high metalicity, suggesting a low dust-to-metals ratio. This figure is taken from Watson et al. (2005).

(β), $\Gamma - 1 = \beta$, which in turn is related to the electron energy distribution index p in any given spectral regime ($\beta = p/2$ if $\nu_c < \nu_X$ and $\beta = (p-1)/2$ if $\nu_c < \nu_X$). The corresponding temporal decay index α_X would be $(3p-2)/4$ and $3(p-1)/4$ respectively before the jet break and p in both spectral regimes after the jet break, according to the standard fireball model for an afterglow expanding in a homogeneous interstellar medium. In the present case, the observed values of α_X are consistent with the $p = 1.42$ and the jet break around 0.06 days after the burst. However, we note that the observed value of the spectral photon index $\Gamma \sim 1.85 \pm 0.03$ (Watson et al., 2005) implies a larger $p \sim 1.7 \pm 0.06$. It should also be noted that from analysis of the same data set of x-ray observations, De Pasquale et al. (2006) infers $\beta = 0.75 \pm 0.15$ for PC mode data after the break at 0.06 days. This β is consistent with $p = 1.42$, we inferred above.

The optical (R-band) afterglow, on the other hand, exhibits a temporal slope $\alpha_R = 0.82$ which, in the commonly encountered spectral regime of $\nu_m < \nu_R < \nu_c$, implies $p = 2.1$. This is different from that inferred for the x-ray afterglow, and indeed regardless of the choice of spectral regimes it is not possible to produce both α_X and α_R from the same underlying power-law energy distribution of injected electrons. One possibility, therefore, is that the optical and the x-ray afterglows originate in physically distinct outflows. We consider two physically distinct components of the outflow, such as the co-axial jets, one having a dominant contribution in the optical and the other in the x-rays, giving rise to the observed afterglow of GRB 050401.

We then fit the full, multi-band light curves of GRB050401 with those predicted by a double jet model using linear least square method. Results of this fit are displayed in Figure 5.4, and the best fit values of various spectral parameters are listed in Table 5.4. We note that the contribution of the narrow jet to the optical afterglow is strongly suppressed due to large extinction. The x-ray afterglow, on

	Narrow Jet	Wider Jet
ν_m(Hz)	$2.0^{+1.2}_{-0.81} \times 10^{13}$	$1.1^{+1.53}_{-0.83} \times 10^{13}$
ν_c(Hz)	$4.1 \pm 0.9 \times 10^{14}$	$5.25^{+30.0}_{-5.0} \times 10^{15}$
$F_{peak}(\mu Jy)$	2140^{+210}_{-230}	1750^{+1050}_{-950}
t_{jet}(day)	0.06 ± 0.03	–
p	1.42 ± 0.02	$2.1^{+0.2}_{-0.11}$
$E(B-V)_{Host}$	4.1	$0.23^{+0.22}_{-0.13}$
χ^2_{dof}(dof)	1.2 (85)	

Table 5.4: Best fit Spectral parameters for the afterglow of GRB 050401 assuming two component jet model described in § 5.5. Light curves generated using these parameters and their subsequent evolution according to the standard fireball model are plotted in Figure 5.4. All the parameters are calculated at 0.01 day after the burst. GRB 050401 was at redshift $z = 2.9$

the other hand, is modified as a sum of the emission from both the jets, with the narrow jet being the dominant contributor. For the narrow jet we find a best fit value of $p = 1.42$. For the wider jet, which dominates the optical afterglow of GRB 050401, we estimate $p = 2.1$. The extinction that the radiation from the narrow jet encounters is fixed at A_v (host) $= 9.1$ as derived from the soft x-ray absorption (Watson et al., 2005), while that for the wide jet is treated as a fit parameter.

5.5.2 Physical Parameters for GRB 050401

Four spectral parameters (ν_a, ν_m, ν_c and F_{peak}) are related to four physical parameters viz. n (number density of the circumburst medium), E (total energy content of the fireball), energy fraction in relativistic electrons ϵ_e and that in magnetic field ϵ_B. The typical value of self absorption frequency ν_a lies in radio-mm waves and hence is best estimated only if the afterglow is well observed in these bands. Unfortunately, the afterglow of GRB 050401 was detected only once at the radio band (Soderberg, 2005)

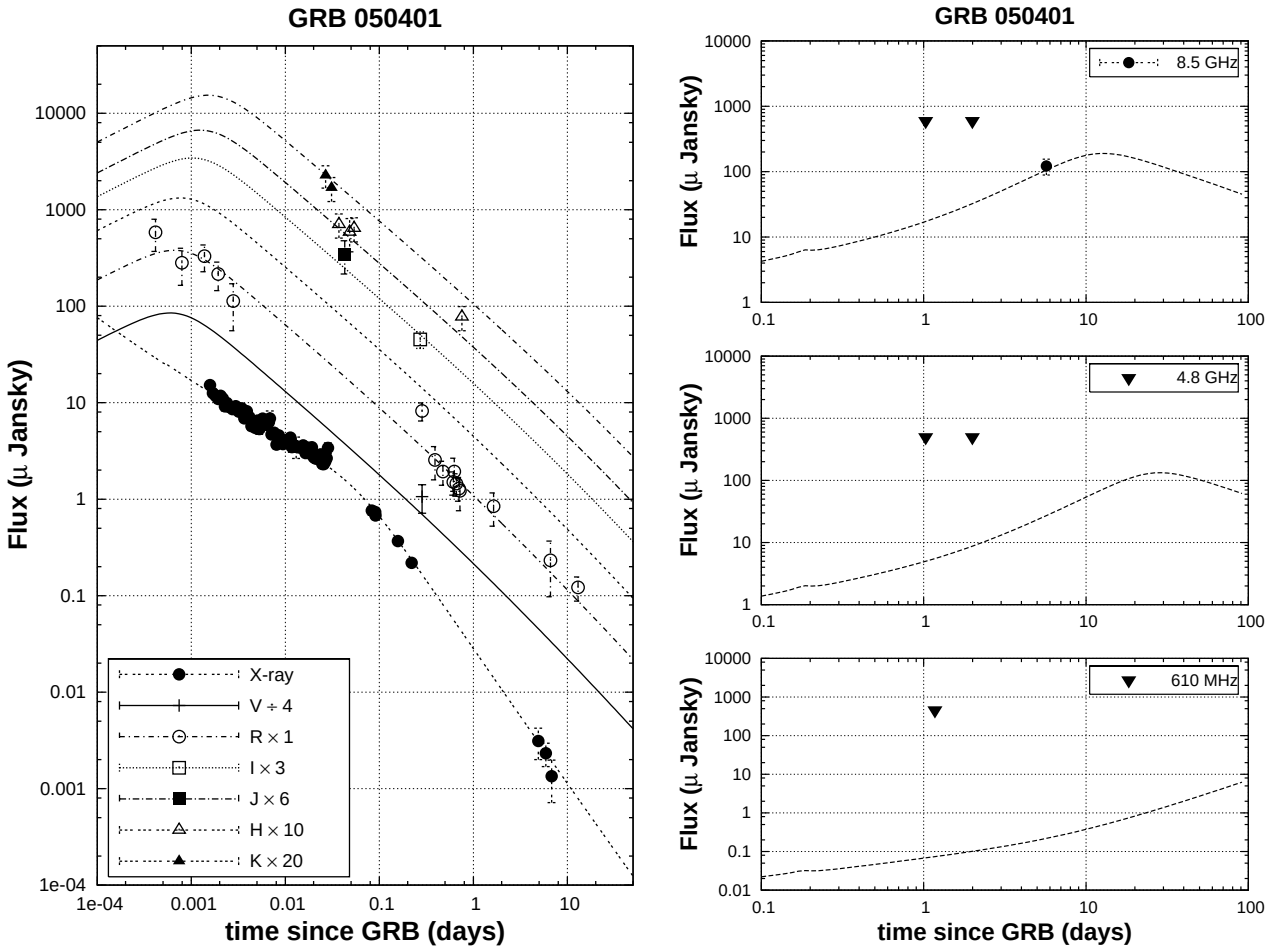

Figure 5.4: The observed optical & x-ray light curves (*left panel*) and radio light curves (*right panel*)of GRB 050401 afterglow compared with the double jet model fit (lines). The steepening of x-ray afterglow light curves at 0.06 day after the burst is explained as a jet break due to the lateral expansion of a narrow jet which has a dominant contribution in x-rays. The surrounding wider jet contributes dominantly in optical. Since, no break in the optical light curves is observed till 13 days after the burst, the wider jet is expected to be $> 29°$. Our best fit model gives the value of electron energy distribution index within the narrow jet to be $p = 1.42$ and that within the wider jet to be $p = 2.1$. The peak in the optical light curves corresponds to the passage of ν_m through the observing band. The radio upper limits are indicated by filled triangles in the right panels. The sole radio detection at 8.5 GHz is indicated by a filled circle. The dashed lines in the right panels are the light curves expected from the best fit spectral parameters. The corresponding frequencies are listed in a rectangle at the top right corner of each box.

	Narrow Jet	Wider Jet
n	$14.7^{+10.5}_{-5.34}$	$20^{+2583}_{-19.3}$
ϵ_e	$(2.3 \pm 0.6) \times 10^{-2}$	$(4^{+6}_{-2}) \times 10^{-2}$
ϵ_B	$5^{+4}_{-2} \times 10^{-4}$	$1^{+9}_{-0.9} \times 10^{-3}$
E^{iso}_{52}	53.23 ± 16.2	$1.34^{+1.36}_{-0.82}$
θ_j	$1.15^\circ \pm 0.15^\circ$	$> 29^\circ$
E^{corr}_{52}	$(1.1 \pm 0.2) \times 10^{50}$	$> 6.5 \times 10^{50}$

Table 5.5: The physical parameters for the afterglow of GRB 050401 assuming a two component jet model described in § 5.5. The quantity E^{iso}_{52} is the isotropic equivalent energy in units of 10^{52} ergs. The corresponding collimation corrected energy is E^{corr}_{52} in units of 10^{52} ergs.

which is not sufficient to determine ν_a accurately. We therefore converted the three remaining spectral parameters into the four physical parameters using $\epsilon_e = \sqrt{\epsilon_B}$ as an additional constraint. The choice of this relation is motivated by Medvedev (2006). The values of ϵ_e and ϵ_B estimated from multi-band model fitting of various GRBs do fall within this relation, though not exactly. When $p < 2.0$, as it is in the present case of narrow jet, a high energy cut-off for the electron energy distribution is required and the expressions for spectral parameters, as given in Wijers and Galama (1999), has to be modified accordingly. The modifications have been provided by Bhattacharya (2001) which we have used for estimating the physical parameters in the present case. We estimate the density of the circumburst medium to be $n \approx 10$ and $\epsilon_e = \sqrt{\epsilon_B} = 0.03$ for both the jets. The physical parameters estimated for both the jets are listed in Table 5.5. Using the E^{iso} and n, and the jet break time in x-rays, $t_j = 0.06$ days, we find the opening angle of the narrow jet to be quite small, 1.15°. Since there is no jet break seen in the optical light curve till ~ 13 days, a lower limit on the opening angle of the wider jet is derived to be 29°. The collimation corrected kinetic energies are $E^K_{wide} > 6.5 \times 10^{50}$ ergs and $E^K_{narrow} = 1.1 \times 10^{50}$ ergs.

5.6 Discussion

5.6.1 Plausible explanation for the large extinction inferred from x-ray absorption

It is now well established from the observations of GRB hosts that long GRBs preferentially occur in massive star forming regions e.g. Woosley and Bloom (2006). The massive star forming regions host large molecular clouds. Typical column densities of cold molecular clouds are $> 10^{22}$ cm^{-2}, densities $100 - 10^4 cm^{-3}$ and sizes ~ 20 pc. Giant molecular clouds are even denser ($10^4 - 10^7$cm^{-3}) and larger (~ 100 pc) (Shore, 2002). It is possible that one such cloud in the host galaxy of GRB 050401 happens to fall along our line of sight which can explain the large extinction inferred from the x-ray spectrum. We consider a possibility of radiation from the double jet of GRB 050401 being obscured by a molecular cloud so aligned that it covers the narrow jet of GRB 050401 completely while the wide jet is partially covered. By changing the fractional coverage of wide jet by the cloud we measured change in the value of reduced χ^2 of the fit. In effect, this amounts to adjusting the intrinsic luminosity of the wide jet upwards with increasing covering factor to match the observed optical flux. This results in the relative contribution of the wide jet to the x-ray afterglow to increase, affecting the fit quality. Keeping all other parameters fixed at their best fit values obtained for zero coverage, we find that a covering fraction of 60% can be accomodated within a range of $\Delta\chi^2/dof = 1$. Beyond this the reduced χ^2 rises sharply and reaches $\Delta\chi^2/dof > 15$ for a covering factor of $\sim 90\%$. The size of the cloud required, for entirely covering the narrow jet of half opening angle $\sim 1.15°$, ranges between $2 - 20$ pc when placed at a distance of $100 - 1000$ pc away from the GRB which is comparable to the observed sizes of cold molecular clouds. Similarly a molecular cloud of about 20 pc dimension seen from a distance of a few tens of

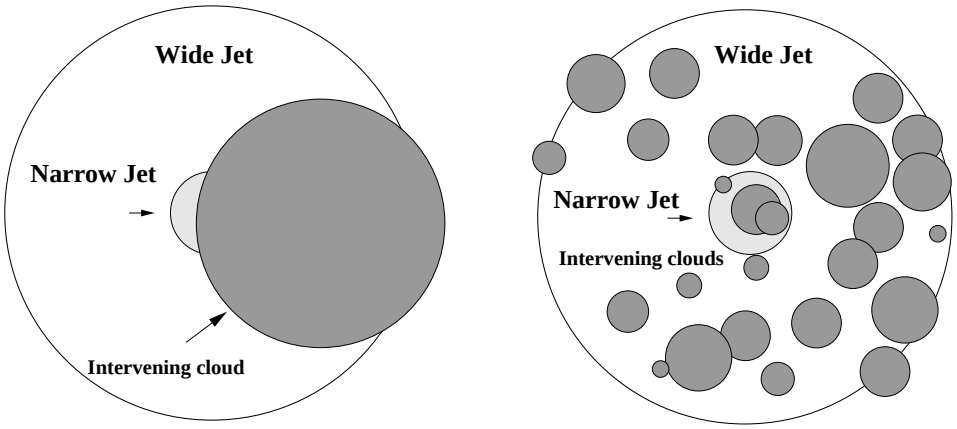

Figure 5.5: The double jet as seen by an observer on the axis of the jets. The bigger unfilled circle is the wide jet, the smaller partially filled circle at the center is the narrow jet and more densly filled circles are the intervening molecular clouds responsible for the observed large extinction. The figure on the left side considers a situation in which one large cloud covers a significant portion of the central narrow jet and partially covers the wide jet. As a result optical radiation from the narrow jet is completely extincted. Most of the optical radiation from the wide jet does not suffer from this extinction. A similar result could be obtained by having a large number of smaller intervening clouds as shown in the figure on the right hand side.

parsecs will occupy angular size as large as the lower limit on the size of the wide jet (29°). It is therefore probable that one such molecular cloud partially obscures our view of GRB 050401. An alternative possibility is that a few smaller molecular clouds of a few parsec size at a distance of a few tens of parsecs, could cover the narrow jet as well as $\leq 60\%$ of the wide jet. These situations are illustrated in Figure 5.5.

5.6.2 GRB 050401 and GRB 030329 : A comparison

The only other GRB whose afterglow has been explained as being due to double jet is the GRB 030329 (Berger et al., 2003; Resmi et al., 2005). Optical and x-ray light curves of GRB 030329 afterglow showed a near simultaneous break at 0.55 day whereas the radio light curves had a break at about 10 days after the burst. Berger et al. (2003) has explained the two breaks as being due to lateral expansion of the two co-axial jets of different opening angles ($\sim 5^\circ$ and $\sim 17^\circ$).

In the case of GRB 050401, afterglow light curves do not show the presence of two different breaks. Instead, absence of a break at optical frequencies till late times ($\sim$ 13 days after the burst) leads us to infer the presence of a wider jet with opening angle larger than 29° while a steep break ($\Delta\alpha \sim 0.8$) at 0.06 day after the burst in x-ray light curve can be explained as a jet break due to lateral expansion of a narrow jet of opening angle 1.15°.

The wider jet of GRB 030329 was estimated to be marginally more energetic than the narrower jet (Berger et al., 2003; Resmi et al., 2005). Similarly, in the case of GRB 050401, we find, that the wider jet is marginally more energetic than the narrower jet.

5.6.3 GRB 050401 and the Ghirlanda Relation :

It has been found that the collimation corrected energies (E_γ) of the GRBs are correlated with the peak energy of the GRB spectrum as measured in the frame of reference of the source (E^{src}_{peak}). This correlation is also called as the Ghirlanda relation (Ghirlanda et al., 2004). Unfortunately, the E^{src}_{peak} for GRB 050401 is not available as it falls outside the energy range of BAT. However, Sato et al. (2007) have used the Konus-Wind spectral data to find E^{obs}_{peak}. From their analysis Sato et al. (2007) finds that in order to satisfy the Ghirlanda relation the afterglow light curve

of GRB 050401 should exhibit a jet break $\sim 10^4$ s after the burst. This lower limit of the allowed range for jet break time is close to the break seen at 0.06 day in the x-ray light curve of GRB 050401, which we interpret as a jet break corresponding to the narrow jet in our model.

Sato et al. (2007) quantifies the Ghirlanda relation as $E^{src}_{peak} = A\, E^{0.706}_{\gamma,52}$ where $E_{\gamma,52}$ is the collimation corrected energy released in γ rays during the burst, in units of 10^{52} ergs. Using a sample of a large number of GRBs Sato et al. (2007) constrains the value of the proportionality constant A : $1950 < A < 4380$. Using the estimated value of $E^{iso}_{\gamma} \sim 10^{54}$ ergs and the 1.15° as the opening angle of the narrow jet in our double jet model, the E_{γ} turns out to be 2×10^{50} ergs. Using $E^{src}_{peak} = 447^{+75}_{-64} keV$ for GRB 050401 as reported by Sato et al. (2007) along with $E_{\gamma} = 2 \times 10^{50}$ ergs we estimate $A = 7076^{+2597}_{-1897}$. This value of A is within 2 σ of $A = 4380$, the higher limit on A obtained considering the sample of GRBs satisfying the Ghirlanda relation.

5.7 Summary

We have reported V, R, I band observations of GRB 050401 afterglow on 1st Apr. 2005. Also, we have modeled the afterglow of GRB 050401 as due to two physically distinct collimated outflows, using re-analysis of *Swift* XRT observations and our own VRI band photometry along with the observations available in the literature, and compared with GRB 030329. Our main conclusions about GRB 050401 are as follows :

1. We showed that the light curves of GRB 050401 afterglow can not be explained under the assumption of continuous energy injection. The flatter decay, which appealed for the continuous energy injection model, can instead be explained by low values of electron energy distribution index p.

2. The afterglow of GRB 050401 can be well fit by the double jet model with the interpretation that the break in the x-ray light curve at ~ 0.06 day after the burst is due to a narrow collimated jet expanding sideways. The obscured optical emission is attributed to a wider jet which did not undergo significant sideways expansion until at least ~ 13 days after the burst.

3. Energies of the two jets are of the same order but somewhat larger for the wider jet.

4. Our interpretation of the break in the x-ray light curve at 0.06 days after the burst as a jet break is consistent with the Ghirlanda relation.

Bibliography

Angelini L., Racusin J.L., Hunsberger S. et al. GRB Coordinates Network, 3161, 1 (2005).

Barbier L., Barthelmy S., Cummings J. et al. GRB Coordinates Network, 3162, 1 (2005).

Berger E., Kulkarni S.R., Pooley G. et al. Nature, 426, 154 (2003).

Bessell M.S., Castelli F. and Plez B. A&A, 333, 231 (1998).

Bhattacharya D. Bulletin of the Astronomical Society of India, 29, 107 (2001).

Chandra P. and Ray A. GRB Coordinates Network, 3178, 1 (2005).

De Pasquale M., Beardmore A.P., Barthelmy S.D. et al. MNRAS, 365, 1031 (2006).

Fynbo J.P.U., Jensen B.L., Hjorth J. et al. GRB Coordinates Network, 3176, 1 (2005).

Ghirlanda G., Ghisellini G. and Lazzati D. ApJ, 616, 331 (2004).

Golenetskii S., Aptekar R., Mazets E. et al. GRB Coordinates Network, 3179, 1 (2005).

Henden A. GRB Coordinates Network, 3454, 1 (2005).

Landolt A.U. AJ, 104, 340 (1992).

Mathis J.S. ARA&A, 28, 37 (1990).

Medvedev M.V. ApJ Lett, 651, L9 (2006).

Meszaros P. and Rees M.J. ApJ Lett, 418, L59+ (1993).

O'Brien P.T., Willingale R., Osborne J. et al. ApJ, 647, 1213 (2006).

Panaitescu A., Mészáros P., Burrows D. et al. MNRAS, 369, 2059 (2006).

Pe'er A., Mészáros P. and Rees M.J. ApJ, 652, 482 (2006).

Price P.A. and McNaught R. GRB Coordinates Network, 3164, 1 (2005).

Rees M.J. and Meszaros P. MNRAS, 258, 41P (1992).

Resmi L., Ishwara-Chandra C.H., Castro-Tirado A.J. et al. A&A, 440, 477 (2005).

Rykoff E.S., Yost S.A., Krimm H.A. et al. ApJ Lett, 631, L121 (2005).

Sakamoto T., Barthelmy S., Barbier L. et al. GRB Coordinates Network, 3173, 1 (2005).

Sari R., Piran T. and Narayan R. ApJ Lett, 497, L17+ (1998).

Saripalli L., Wu K., Ghosh K.K., Swartz D.A. and Tennant A.F. GRB Coordinates Network, 3177, 1 (2005).

Sato G., Yamazaki R., Ioka K. et al. ApJ, 657, 359 (2007).

Schlegel D.J., Finkbeiner D.P. and Davis M. ApJ, 500, 525 (1998).

Shore S.N. The tapestry of modern astrophysics (The tapestry of modern astrophysics/ Steven N. Shore. New York: John Wiley & Sons, c2003., 2002).

Soderberg A.M. GRB Coordinates Network, 3187, 1 (2005).

Stetson P.B. PASP, 99, 191 (1987).

Watson D., Fynbo J.P.U., Ledoux C. et al. ArXiv Astrophysics e-prints (2005).

Wijers R.A.M.J. and Galama T.J. ApJ, 523, 177 (1999).

Willingale R., O'Brien P.T., Osborne J.P. et al. ArXiv Astrophysics e-prints (2006).

Woosley S.E. and Bloom J.S. ARA&A, 44, 507 (2006).

Zhang B., Fan Y.Z., Dyks J. et al. ApJ, 642, 354 (2006).

Zhang B. and Mészáros P. ApJ Lett, 552, L35 (2001).

Zhang B. and Mészáros P. ApJ, 566, 712 (2002).